Nano World Journal

https://doi.org/10.17756/nwj.2023-s5-045

Research Article

Open Access

Synergistic Properties of $(Au_2V)_{0.01}(V_2O_5)_{0.99}$ Composite: Synthesis, Characterization, and Enhanced Functionalities

Ashish K. Kumawat[1], Kriti Kumari[1], Bhakti Tripathi[1], Satyapal Rathore[2] and Rashi Nathawat[1*]

[1]Funtional Ceramic and Smart Material Lab, Department of Physics, Manipal University, Jaipur, Rajasthan, India
[2]Department of Physics, Cluster University of Jammu, Jammu and Kashmir, India

***Correspondence to:**
Rashi Nathawat
Funtional Ceramic and Smart Material Lab, Department of Physics, Manipal University, Jaipur, Rajasthan, India.
E-mail: rashi.nathawat@gmail.com

Received: October 20, 2023
Accepted: December 22, 2023
Published: December 28, 2023

Citation: Kumawat AK, Kumari K, Tripathi B, Rathore S, Nathawat R. 2023. Synergistic Properties of $(Au_2V)_{0.01}(V_2O_5)_{0.99}$ Composite: Synthesis, Characterization, and Enhanced Functionalities. *NanoWorld J* 9(S5): S231-S235.

Published by United Scientific Group

Abstract

The synergistic combination of distinct materials to create composite structures has garnered significant interest in various scientific disciplines. In this study, we present the synthesis and characterization of a composite material composed of Au_2V (Gold vanadate) and V_2O_5 (Vanadium pentoxide). The unique properties of V_2O_5, including its semiconducting behavior. The integration of Au_2V with V_2O_5 offers the potential to create a composite material. The synthesis methodology, involving the controlled formation is detailed. Comprehensive characterization through techniques X-ray diffraction (XRD), Field emission-scanning electron microscopy (FE-SEM), Fourier-transform infrared spectroscopy (FTIR), Ultraviolet-Visible spectroscopy (UV-Vis) and Photoluminescence spectroscopy (PL) have been performed. This study contributes to the understanding of composite materials. The $(Au_2V)_{0.01}(V_2O_5)_{0.99}$ composite's tailored properties and improved catalytic activity hold promise for future applications in green and sustainable catalysis, paving the way for innovative solutions in diverse chemical processes.

Keywords

Composite, Gold vanadate, Hydrothermal, 3D structure

Introduction

In recent years, the field of nanomaterials has witnessed remarkable advancements, leading to the development of innovative materials with tailored properties for various applications. Among these, metal oxide composites have attracted considerable attention due to their synergistic properties arising from the combination of distinct materials. In particular, the integration of noble metals with metal oxides has shown great promises in catalytic applications owing to their enhanced reactivity, selectivity, and stability. M-V_2O_5 (Metal-modified vanadium oxide) refers to a type of material where V_2O_5 is chemically modified by incorporating or introducing other metal elements into its structure [1-3]. This modification can alter the material's properties, such as its catalytic, electrical, and optical characteristics. The metal elements can influence the vanadium oxide's behavior and reactivity, making it suitable for various applications [4-6]. Metal modification of vanadium oxide can occur through different methods, including doping, impregnation, co-precipitation, sol-gel synthesis, and more. The choice of the metal element and the modification process depends on the desired properties and applications of the modified material. M-V_2O_5 catalysts can be used in various industrial processes, such as the oxidation of organic compounds, removal of pollutants from air and water, and the synthesis of chemical [7, 8]. M-V_2O_5 can be used in energy storage systems, such as lithium-ion batteries and supercapacitors, to improve the overall performance and efficiency of the

devices. These materials can also be employed as gas sensors for detecting specific gases, such as nitrogen dioxide or hydrogen, due to their sensitivity to changes in gas concentration [3, 9]. Additionally, in electrochromic devices for applications like smart windows and displays [10, 11]. M-V_2O_5 can be utilized as photocatalysts to drive chemical reactions using light energy, which finds applications in environmental remediation and solar fuel production [12-14]. Thermochromic materials change color with temperature variations. M-V_2O_5 can be incorporated into thermochromic coatings for applications in temperature-sensitive paints or coatings. The choice of the metal modifier, its concentration, and the modification method will greatly influence the resulting properties of the M-V_2O_5 material. Research and development in this field continue to explore novel materials with enhanced performance for various technological applications. The ionic doping can increase the sensitivity of the metal oxide gas sensor due to the introduction of impurities and surface defects. One-dimensional vanadium oxide nanostructures have gained attention due to their improved adsorption and surface reaction kinetics [15]. These rods-like structures are promising for detecting various gases. Intercalation of metal ions into the layered structure of vanadium oxide can enhance sensitivity and detecting abilities. In this work, gold modified vanadium oxide (GVO) rods-like structures synthesized via hydrothermal process. The structural and optical properties of $(Au_2V)_{0.01}(V_2O_5)_{0.99}$ composite were studied in details.

Experimentation

Materials and method

The standard sol-gel assisted hydrothermal process was utilized to synthesis of $(Au_2V)_{0.01}(V_2O_5)_{0.99}$ composite. The synthesis steps shown in figure 1. In standard process, vanadium pentoxide (V_2O_5, ≥98%, Sigma Aldrich), hydrogen peroxide (H_2O_2 30%, Merck) and gold chloride ($AuCl_3$, ≥99%, Sigma Aldrich) were used as a precursor. The partially dissolved solution was prepared by adding 1 g V_2O_5 in 100 ml DI water with 30% concentrated H_2O_2 at constant stirring of 400 rpm to prepared required solution. Then stoichiometric amount of $AuCl_3$ was added at the same parameters. Furthermore, the solution was shifted to 500 ml Teflon container, locked in Stainless Steel autoclave, and kept at 180 °C for 24 h. The precipitate was collected and washed multiple times with DI water and ethanol respectively and dried at ambient temperature. The as-prepared composite $(Au_2V)_{0.01}(V_2O_5)_{0.99}$ (GVO) was then utilized for further physicochemical characterizations.

Characterization

The as-prepared composite, structurally charecterised by advance techniques. Rigaku Ultima-IV diffractometer with Cu Kα line (λ = 0.154 nm) used for XRD and JEOL JSM-7610F Plus used for FE-SEM. Optical studies of materials were performed through UV-Vis spectra (350 - 800 nm) using a Shimadzu UV-2600 spectrophotometer and PL specra using Horiba FluoroMax-4 spectrometer. The FTIR spectrometer (Bruker, Alpha) was used in a spectral range from 500 - 4000 cm^{-1} for studies of chemical bonding spectra.

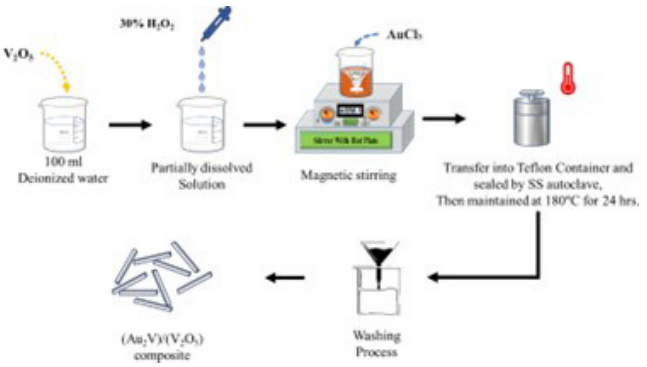

Figure 1: Schematic diagram of steps wise synthesis process.

Results and Discussion

XRD analysis

The identification of phase purity and structural compositions of pure V_2O_5 and GVO composite analysed by X'Pert Highscore Plus software. The XRD pattern of V_2O_5 and GVO were represented in figure 2. V_2O_5 is in highly crystalline phase proved from the high intentional peaks. The observed data matched with JCPDS card no. 01-072-0598 which attributed to V_2O_5 is in an orthorhombic phase. The XRD pattern of GVO matched with two JCPDS card no. 03-065-7653 and of V_2O_5. The composite exist in two phases of Au_2V (gold vanadate) is 1% and V_2O_5 in 99%. The higher international peak shows shifting to higher 2θ° due to tensile strain. Figure 3 shows W-H plots of V_2O_5 and GVO. The positive slop of linear fitting in W-H plots make manifest tensile strain. The tensile strain increased two times in GVO compaired to V_2O_5. The crystallite size evaluated by the Debye-Scherrer is shown in table 1. The crystallite size incresed in GVO sample [4].

FE-SEM analysis

The surface morphology of pure V_2O_5 and GVO

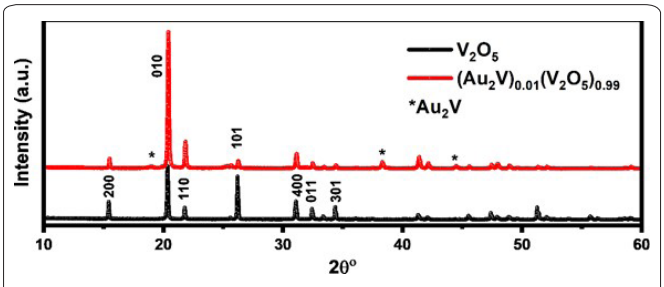

Figure 2: XRD plot of pure V_2O_5 and GVO.

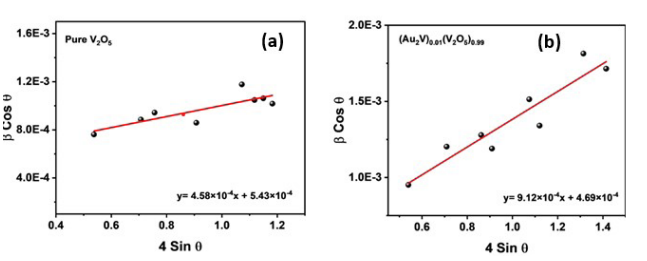

Figure 3: W-H plots of **(a)** pure V_2O_5 and **(b)** GVO.

Table 1: Calculated crystallite size by Debye-Scherrer and Willamson-Hall (W-H) and micro-strain of V_2O_5 and GVO.

Sample	DD-S (nm)	Strain
Pure V_2O_5	15.89	4.58×10^{-4}
GVO	16.37	9.12×10^{-4}

composite are shown in figure 4a and figure 4b, respectvely. The FE-SEM image of V_2O_5 composite demonstrate grains like microstructures of 720 nm in average size. The surface morphology was changed into 3D rod like structures. The change in morphology from a grain-like structure to a rod like structure might be attributed to specific conditions such as temperature, pressure, reaction time, precursor and concentrations, during the hydrothermal process. The histogram reveals avarege width size of rods ~600 nm. The avrage length of rods is ~8 µm. Resulting, the aspect ratio estimated about the value of 13.33. The aspect ratio of conductive rod in a composite material can influence its electrical conductivity result in promising the gas sensing application in further studies.

PL spectra

The room temperature PL spectra of pristine V_2O_5 and GVO shown in figure 5. The PL intensity of rods-like structures is strongly influenced by synthesis method and crystal structure. The PL spectrum was recorded in the range of 510 - 650 nm at an excitation wavelength of 350 nm. The wide emission spectra of V_2O_5 deconvoluted which attributed to indirect inter-band transition at 567.59 nm, while the emission band agree with to mid-state energy states transitions at 613.23 nm [16-19]. The emission peaks are appeared narrow in the composite. Microrods typically have more uniform dimensions compared to irregularly shaped grains. This uniformity can lead to a narrower emission peak, as the rods-like structures have more consistent bandgap energies. GVO structures might exhibit higher crystalline quality compared to grains, which can result in sharper and narrower emission peaks. Fewer defects and grain boundaries mean fewer energy levels within the bandgap, leading to a more well-defined emission energy. Resulting, the FWHM (Full width half maxima) values decreased up to 10.07 for inter-band emission and 11.98 for defect emission. Generally, oxygen vacancies are responsible for defect emission [20-22]. The ratio of FWHM values of inter-band transition and defect emission increased in composite sample as compared to pristine sample. It is evident that the intensity of band emission increases with substitution of Au_2V in V_2O_5. The relative positions and FWHM values of mid-state transition with inter-band transition is summarized in table 2. Both peaks are shifted to higher wavelength side which showing indication for band gap tunning.

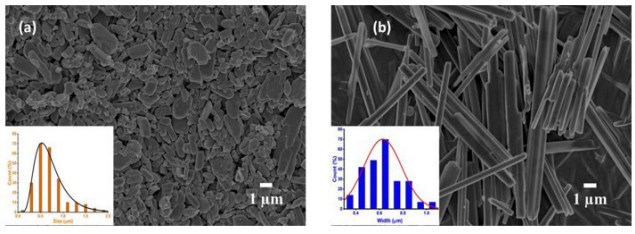

Figure 4: FE-SEM images of **(a)** pure V_2O_5 and **(b)** GVO.

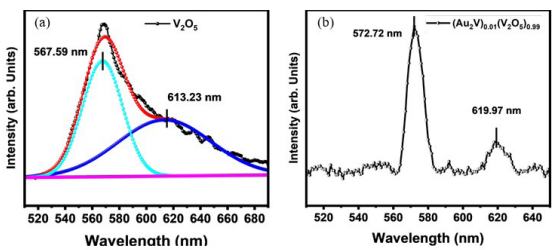

Figure 5: PL spectra of **(a)** V_2O_5 and **(b)** GVO.

UV-Vis analysis

Figure 6a repersents absorption spectra of pure V_2O_5 and GVO. The absorption edge extends at 550 nm due to Π- Π* transition [23, 24]. The absorbance spectra appeared same in range of 400 - 550 nm. Which exhibits the existance of V_2O_5 in the composite, also confirmed by XRD analysis. The fundamental absorption edge was observed hypsochromic effect in composite samples due presence of Au_2V. The Kubelka–Munk function was used to calculate energy bandgap, shown in figure 6b (Tauc plot) [25]. Tauc graph plotted between $[F(R\infty)\ x\ h\nu]n$ vs energy (eV). Where $h\nu$ is incident photon energy and n is the constant value of 1/2 for indirect bandgap. The optical band gaps were calculated by linearly fitting of Tauc plots. The calculated value of pure V_2O_5 and GVO band gap were 2.10 eV and 1.78 eV, respectively [26]. The GVO is lower bandgap material as compare to pure V_2O_5 [27]. The band gap redused by the gold modification due to formation of the new meta energy states between HOMO–LUMO energy gap of V_2O_5.

FTIR analysis

The FTIR spectra of pure V_2O_5 and GVO have been

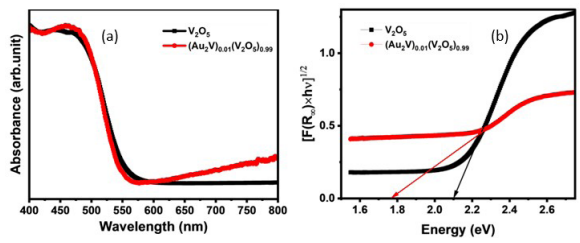

Figure 6: (a) Absorbance spectra and **(b)** Tauc plot of pure V_2O_5 and GVO.

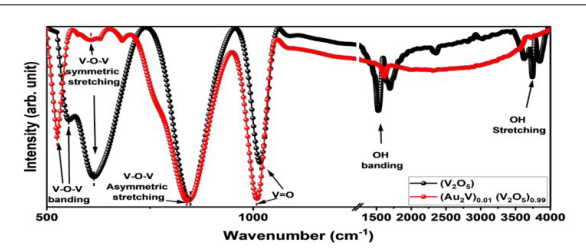

Figure 7: FTIR spectra of pure V_2O_5 and GVO.

Table 2: Peak positions with FWHM values of PL spectra.

	Inter-band emission		Defect emission		
Sample	Position (nm)	FWHM (W_i)	Position (nm)	FWHM (W_d)	Ratio (W_i/W_d)
V_2O_5	567.59	35.01	613.23	81.23	0.43

Table 3: Peak positions in fingerprint region of FTIR spectra.

Sample	Pure V_2O_5	GVO
V-O-V bending	553.21	524.55
V-O-V symmetric stretching	615	603.25
V-O-V asymmetric stretching	846.04	841.55
V=O	1016.5	1010

recorded in figure 7 in the range of 400 - 4000 cm^{-1}. The spectra can be divided in to two regions. First is the fingerprint region in range from 500 cm^{-1} to 1500 cm^{-1} and second is functional group region in range from 1500 cm^{-1} to 4000 cm^{-1}. In FTIR spectra, banding, stretching, and vibrations bonds were seen in fingerprint region [28, 29]. The signature peak of V=O bond at about 1016.47 cm^{-1} and 1009.96 cm^{-1} is clearly appeared in pure V_2O_5 and GVO [30]. The V-O-V bending, symmetric and asymmetric stretching vibrations appear in range of 524 - 554 cm^{-1}, 603 - 615 cm^{-1}, and 841 - 847 cm^{-1}, respectively. The peaks are shifted to lower wavenumber, reveals that the mass of the molecules, and inter molecular forces increased in composite. Apart from this, composites usually are matrix material that holds other components together. The interactions between the matrix and the embedded materials can lead to shifts in vibrational modes and consequently to low-frequency shifts. The vibration peak positions are summarized in table 3. The peaks of OH bending and stretching are appeared in pure V_2O_5 due to moisture [31].

Conclusion

In this study, we have successfully synthesized and characterized the novel composite $(Au_2V)_{0.01}(V_2O_5)_{0.99}$. The integration of these distinct components has led to the creation of a composite with band gap engineering activity, providing a platform for advanced functional applications in photocataly activity and gas sensing. The synthesis process has been shown to influence the structural and morphological properties of the composite. The controlled formation of Au_2V and its integration with V_2O_5 have been successfully achieved, as confirmed via advanced characterization techniques such as XRD, FE-SEM, FTIR, PL, and UV-Vis. The characterization of the GVO have yielded a material with remarkable bandgap potential.

Acknowledgements

The Authors would like to express special thanks to Sophisticated Analytical Instrument Facility (SAIF) and Central Analytical Facilities (CAF,) Manipal University Jaipur, for the provisions of FESEM, XRD, UV-Vis and FTIR facilities; respectively for characterization. RN acknowledges the award of the Enhanced Seed Grant Project No. (EF/2019-21/QE04-03) to her at Manipal University Jaipur, Jaipur. SSR would like to acknowledge the Science and Engineering Research Board (SERB), Govt. of India for financial support under sanctioned project no. ECR/2017/002691.

Conflict of Interest

The authors declare that they have no known competing financial interests or personal relationships that could have appeared to influence the work reported in this paper.

References

1. Kumawat AK, Rathore SS, Singh S, Nathawat R. 2023. Structural transition and photoluminescence behavior of $(V_2O_5)_{1-x}(Ag_{0.33}V_2O_5)_x$ (x=0 to 0.1) nanocomposites. *Results Chem* 5: 100802. https://doi.org/10.1016/j.rechem.2023.100802
2. Whittaker L, Wu TL, Patridge CJ, Sambandamurthy G, Banerjee S. 2011. Distinctive finite size effects on the phase diagram and metal–insulator transitions of tungsten-doped vanadium(IV) oxide. *J Mater Chem* 21(15): 5580-5592. https://doi.org/10.1039/c0jm03833d
3. Zakharova GS, Liu Y, Enyashin AN, Yang X, Zhou J, et al. 2018. Metal cations doped vanadium oxide nanotubes: synthesis, electronic structure, and gas sensing properties. *Sens Actuators B Chem* 256: 1021-1029. https://doi.org/10.1016/j.snb.2017.10.042
4. Takeuchi KJ, Marschilok AC, Davis SM, Leising RA, Takeuchi ES. 2001. Silver vanadium oxides and related battery applications. *Coord Chem Rev* 219: 283-310. https://doi.org/10.1016/S0010-8545(01)00340-X
5. Fieldhouse N, Pursel SM, Horn MW, Bharadwaja SS. 2009. Electrical properties of vanadium oxide thin films for bolometer applications: processed by pulse dc sputtering. *J Phys D Appl Phys* 42(5): 055408. https://doi.org/10.1088/0022-3727/42/5/055408
6. Kianfar E. 2019. Recent advances in synthesis, properties, and applications of vanadium oxide nanotube. *Microchem J* 145: 966-78. https://doi.org/10.1016/j.microc.2018.12.008
7. Pirsa S. 2017. Chemiresistive Gas Sensors Based on Conducting Polymers. In Ahmadi MT, Ismail R, Anwar S (eds) Handbook of Research on Nanoelectronic Sensor Modeling and Applications. IGI Global, pp 150-180.
8. Pandey S. 2016. Highly sensitive and selective chemiresistor gas/vapor sensors based on polyaniline nanocomposite: a comprehensive review. *J Sci Adv Mater Devices* 1(4): 431-453. https://doi.org/10.1016/j.jsamd.2016.10.005
9. Tang H, Yan M, Zhang H, Li S, Ma X, et al. 2006. A selective NH_3 gas sensor based on Fe_2O_3–ZnO nanocomposites at room temperature. *Sens Actuators B Chem* 114(2): 910-915. https://doi.org/10.1016/j.snb.2005.08.010
10. Li B, Yao J, Tian S, Fang Z, Wu S, et al. 2020. A facile one-step annealing route to prepare thermochromic W doped VO_2 (M) particles for smart windows. *Ceram Int* 46(11): 18274-18280. https://doi.org/10.1016/j.ceramint.2020.05.042
11. Salamati M, Kamyabjou G, Mohamadi M, Taghizade K, Kowsari E. 2019. Preparation of TiO_2@W-VO_2 thermochromic thin film for the application of energy efficient smart windows and energy modeling studies of the produced glass. *Constr Build Mater* 218: 477-482. https://doi.org/10.1016/j.conbuildmat.2019.05.046
12. Jayaraj SK, Sadishkumar V, Arun T, Thangadurai P. 2018. Enhanced photocatalytic activity of V_2O_5 nanorods for the photodegradation of organic dyes: a detailed understanding of the mechanism and their antibacterial activity. *Mater Sci Semicond Process* 85: 122-133. https://doi.org/10.1016/j.mssp.2018.06.006
13. Sameie H, Alvani AS, Naseri N, Du S, Rosei FJ. 2018. First-principles study on ZnV_2O_6 and $Zn_2V_2O_7$: two new photoanode candidates

for photoelectrochemical water oxidation. *Ceram Int* 44(6): 6607-6613. https://doi.org/10.1016/j.ceramint.2018.01.064

14. Le TK, Kang M, Kim SW. 2019. Relation of photoluminescence and sunlight photocatalytic activities of pure V_2O_5 nanohollows and V_2O_5/RGO nanocomposites. *Mater Sci Semicond Process* 100: 159-166. https://doi.org/10.1016/j.mssp.2019.04.047
15. Ren J, Wang W, Shang M, Sun S, Zhang L, et al. 2010. Photocatalytic activity of silver vanadate with one-dimensional structure under fluorescent light. *J Hazard Mater* 183(1-3): 950-953. https://doi.org/10.1016/j.jhazmat.2010.07.108
16. Margoni MM, Mathuri S, Ramamurthi K, Babu RR, Sethuraman K. 2017. Sprayed vanadium pentoxide thin films: influence of substrate temperature and role of HNO_3 on the structural, optical, morphological and electrical properties. *Appl Surf Sci* 418: 280-290. https://doi.org/10.1016/j.apsusc.2017.02.039
17. Mjejri I, Etteyeb N, Sediri F. 2014. Mesoporous vanadium oxide nanostructures: hydrothermal synthesis, optical and electrochemical properties. *Ceram Int* 40(1): 1387-1397. https://doi.org/10.1016/j.ceramint.2013.07.020
18. Le TK, Kang M, Kim SW. 2019. Room-temperature photoluminescence behavior of α-V_2O_5 and mixed α-β phase V_2O_5 films grown by electrodeposition. *Mater Sci Semicond Process* 94: 15-21. https://doi.org/10.1016/j.mssp.2019.01.026
19. Kang M, Kim SW, Hwang Y, Um Y, Ryu JW. 2013. Temperature dependence of the interband transition in a V_2O_5 film. *AIP Adv* 3(5): 052129. https://doi.org/10.1063/1.4808021
20. Tsai MT, Chang YS, Chou YH, Tsai KM. 2014. Photoluminescence of titanium-doped zinc spinel blue-emitting nanophosphors. *J Solid State Chem* 214: 86-90. https://doi.org/10.1016/j.jssc.2013.10.019.
21. Mahanti SD, Hoang K, Ahmad S. 2007. Deep defect states in narrow band-gap semiconductors. *Phys B Condens Matter* 401: 291-295. https://doi.org/10.1016/j.physb.2007.08.169
22. Bergerud AJ. 2016. Phase stability and transformations in vanadium oxide nanocrystals. University of California, Berkeley. (Doctoral Dissertation)
23. Kumawat AK, Nathawat R, Rathore SS, Mukhopadhyay AK. 2021. Band gap tuning possibilities in vanadium oxide. *Mater Today Proc* 43: 2939-2943. https://doi.org/10.1016/j.matpr.2021.01.291
24. Nathawat R, Kumawat AK, Rathore SS, Mukhopadhyay AK, Kabra K. 2021. Effect of heat treatment on band gap of V_2O_5. *Sumy State University* 13(5): 1030. https://doi.org/10.21272/jnep.13(1).01030
25. Chen Q. 2020. Optical linear & nonlinearity and Faraday rotation study on V_2O_5 nanorod doped glass and glass-ceramic: impact of optical basicity. *J Alloys Compd* 836: 155490. https://doi.org/10.1016/j.jallcom.2020.155490
26. Kundu S, Satpati B, Kar T, Pradhan SK. 2017. Microstructure characterization of hydrothermally synthesized PANI/V_2O_5.nH_2O heterojunction photocatalyst for visible light induced photodegradation of organic pollutants and non-absorbing colorless molecules. *J Hazard Mater* 339: 161-173. https://doi.org/10.1016/j.jhazmat.2017.06.034
27. Ranjan P, Chakraborty T. 2020. Theoretical Analysis of Au-V Nanoalloy Clusters: A Density Functional Approach. In Singh SB, Vakhrushev AV, Haghi AK (eds) Materials Physics and Chemistry. Apple Academic Press, New York.
28. Nandiyanto AB, Oktiani R, Ragadhita R. 2019. How to read and interpret FTIR spectroscope of organic material. *Indones J Sci Technol* 4(1): 97-118. https://doi.org/10.17509/ijost.v4i1.15806
29. Sabah FA, Razak IA, Kabaa EA, Zaini MF, Omar AF. 2020. Characterization of hybrid organic/inorganic semiconductor materials for potential light emitting applications. *Opt Mater* 107: 110117. https://doi.org/10.1016/j.optmat.2020.110117
30. Farahmandjou M, Abaeiyan N. 2017. Chemical synthesis of vanadium oxide (V_2O_5) nanoparticles prepared by sodium metavanadate. *J Nanomed Res* 5(1): 00103. https://doi.org/10.15406/jnmr.2017.05.00103
31. Baker AG. 2019. The study of optical energy gap, refractive index, and dielectric constant of pure and doped polyaniline with HCl and H_2SO_4 acids. *ARO Sci J Koya Univ* 7(1): 47-52. https://doi.org/10.14500/aro.10483